Biomedical Microdevices (2017) 19: 49
http://dx.doi.org/10.1007/s10544-017-0190-3, *Manuscript as accepted*

Hybrid intracerebral probe with integrated bare LED chips for optogenetic studies

Suleman Ayub[1], Luc J. Gentet[2,3], Richárd Fiáth[4,5], Michael Schwaerzle[1,6], Mélodie Borel[2,3], François David[2,3], Péter Barthó[4,7], István Ulbert[4,5], Oliver Paul[1,6] and Patrick Ruther[1,6]

[1]University of Freiburg, Department of Microsystems Engineering (IMTEK) Freiburg, Germany

[2]Team Waking, Lyon Neuroscience Research Center (CNRL), INSERM-U1028, CNRS-UMR 5292, Bron, France

[3]University Lyon 1, Lyon, France

[4]Institute of Cognitive Neuroscience and Psychology, Research Centre for Natural Sciences, Hungarian Academy of Sciences, Magyar tudósok körútja 2, Budapest, Hungary

[5]Faculty of Information Technology and Bionics, Pázmány Péter Catholic University, Práter utca 50/A, Budapest, Hungary

[6]Cluster of Excellence BrainLinks-BrainTools, University of Freiburg, Freiburg, Germany

[7]MTA TTK NAP B Sleep Oscillations Research Group, Magyar tudósok körútja 2, Budapest, Hungary

Abstract

This article reports on the development, i.e., the design, fabrication, and validation of an implantable optical neural probes designed for in vivo experiments relying on optogenetics. The probes comprise an array of ten bare light-emitting diode (LED) chips emitting at a wavelength of 460 nm and integrated along a flexible polyimide-based substrate stiffened using a micromachined ladder-like silicon structure. The resulting mechanical stiffness of the slender, 250-µm-wide, 65-µm-thick, and 5- and 8-mm-long probe shank facilitates its implantation into neural tissue. The LEDs are encapsulated by a fluropolymer coating protecting the implant against the physiological conditions in the brain. The electrical interface to the external control unit is provided by 10-µm-thick, highly flexible polyimide cables making the probes suitable for both acute and chronic in vivo experiments. Optical and electrical properties of the probes are reported, as well as their in vivo validation in acute optogenetic studies in transgenic mice. The depth-dependent optical stimulation of both excitatory and inhibitory neurons is demonstrated by altering the brain activity in the cortex and the thalamus. Local network responses elicited by 20-ms-long light pulses of different optical power (20 µW and 1 mW), as well as local modulation of single unit neuronal activity to 1-s-long light pulses with low optical intensity (17 µW)

are presented. The ability to modulate neural activity makes these devices suitable for a broad variety of optogenetic experiments.

Keywords Optical probe, neural probes, LEDs, optogenetics, in vivo application

1 INTRODUCTION

Neural engineering has been instrumental in addressing the challenges lying in the way of understanding the functionality of brain as well as analyze its potential dysfunctions (Crick 1979). At the level of neuronal circuits, these challenges have been addressed in particular by recording the electrophysiological response of brain (Wiest et al. 2007) to external stimuli or by functional electrical stimulation (Hanson et al. 2007). For these purposes, external electrodes, e.g. for electroencephalography (EEG), and implantable depth or surface electrodes, e.g. for electrocorticography (ECoG), have been applied. For the fabrication of neural systems with high-density electrodes, precision machining is increasingly being replaced by microelectromechanical systems (MEMS) technologies (Alivisatos et al. 2013). In general, these MEMS-based devices rely on polymers (Stieglitz et al. 2005) or silicon (Herwik et al. 2009; Wise et al. 2008) as substrate materials, with the latter enabling the co-integration of electrodes with complementary metal-oxide semiconductor (CMOS) integrated circuits (Ruther and Paul 2015) performing data preprocessing and multiplexing tasks.

In this context, the field of optogenetics has emerged as a new and highly innovative experimental approach to direct interaction with neurons: rather than electrical signals, light is used to stimulate or inhibit brain activity (Boyden et al. 2005). The optogenetic approach enables a cell-type specific interaction with neural tissue with high temporal and spatial resolution. As a result of targeted viral transfection used among other methods, neuronal cells express light sensitive molecules termed opsins in their cell membranes. As an example, so-called channelrhodopsins, e.g. channelrhodopsin-2 (ChR2) (Nagel et al. 2003), and halorhodopsins, e.g. natromonas pharaonis halorhodopsin (NpHR) (Zhang et al. 2007), increase or, respectively, silence neural

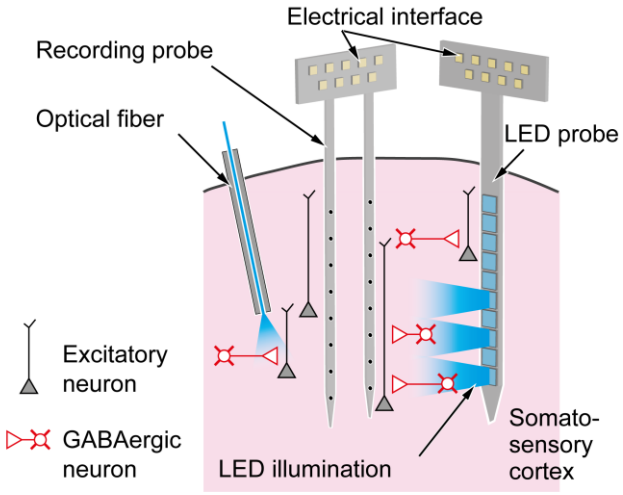

Fig. 1: Schematic of an LED-based optical probe (right) implanted next to a recording probe (middle), in comparison with an optical fiber providing a single optical stimulation site (left).

activity under the influence of light. The reaction strength of opsins can be tailored for different optical wavelengths: ChR2 and NpHR for example are most sensitive at 470 nm (Boyden et al. 2005) and 590 nm (Gradinaru et al. 2010), respectively.

Besides these optogenetic innovations, the development of implantable, miniaturized technical interfaces for the localized delivery of light and recording of neural activity has emerged as a lively research topic in the field of neuroengineering (Alt et al. 2017). In early in vivo optogenetic experiments, optical fibers coupled to external light sources were applied (Yizhar et al. 2011). The depth control of the optical stimulation was achieved by translating the fiber within the neural tissue. However, the fiber approach has inherent disadvantages such as the risk of significant tissue damage, a time-consuming procedure for fiber repositioning, and the stiffness of the optical connection of the test subject to the external light source, which might negatively influence the behavior of supposedly freely behaving animals during in vivo experiments. A typical experimental scenario applicable with these devices using a separately implanted recording probe is illustrated in Fig. 1 (right side) in comparison with the standard approach using a glass fiber (left side).

The limitation of singular optical stimulation per fiber was tackled by introducing multiple optical output ports into a conical optical fiber tip using a sophisticated fabrication technology (Pisanello et al. 2014). The selection of the different optical ports is achieved by coupling the light from the external source under defined angles into the fiber. The external hardware used for light modulation is relatively bulky and the optical connection to the test subject remains stiff. The consequent next step in view of optical probe development therefore relies on the integration of light sources close to or directly onto the implantable technical interface. Hence, the connection to the external instrumentation can rely on potentially more flexible electrical cables or on wireless data transmission.

A first approach in this direction has combined a Silicon (Si)-based neural probe comprising an integrated polymeric waveguide with a packaged laser diode (Park et al. 2011). In order to get rid of the relatively large diode housing, other groups have integrated bare laser diode chips onto neural probes containing integrated optical waveguides (Kampasi et al. 2016; Schwaerzle et al. 2017). These approaches enable the all-electrical control of the optical probes. Alternative probe concepts have been based on thin-film LEDs integrated on flexible substrates using transfer printing (Kim et al. 2013) and wafer-level bonding (Goßler et al. 2014) technologies, respectively. The latter approach was adapted by us to integrate the miniaturized micro-LEDs (µLEDs) on penetrating Si-based probe shanks (Ayub et al. 2016). A different solution applies GaN-based LED layers grown on Si substrates and structured into µLEDs (Scharf et al. 2016; Wu et al. 2015). The optical probes based on either laser diodes or LEDs may further include electrical recording sites along the probe shank for monitoring electrical brain activity close to the optical stimulation sites (Kampasi et al. 2016; Schwaerzle et al. 2013; Wu et al. 2015).

Although the thin-film LED approach enables highly miniaturized light sources to be integrated along the probe shanks, these technology-driven approaches have drawbacks. First, in view of the costs of GaN-based LED-wafers (sapphire or Si), the technology is per se relatively expensive for prototyping purposes. Second, unless the transfer printing technology (Kim et al. 2013) is used, each LED will have the same emission wavelength, thus limiting the flexibility of probe design and application. In order to address this limitation, we have recently presented a new optical probe variant (Ayub et al. 2015) integrating commercially available, bare LED chips into a penetrating optical probe. The device is based on a flexible polymer substrate stiffened using a ladder-like Si structure realized using MEMS technologies. This article describes in detail the probe development, the system characterization, and the in vivo validation by a depth-dependent optical stimulation of the cortex and thalamus of anesthetized transgenic mice.

2 MATERIALS AND METHODS

2.1 Device design

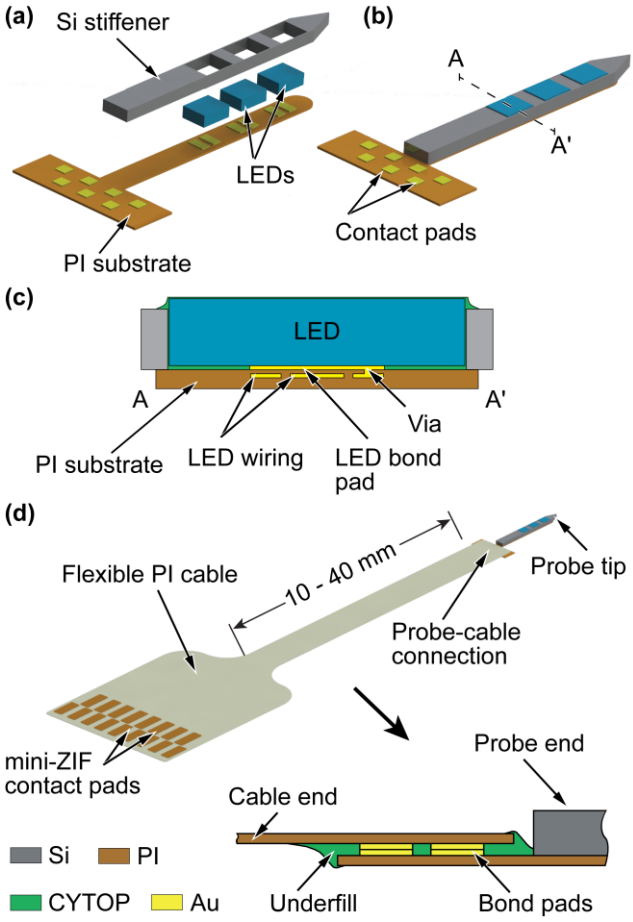

Fig. 2: Probe and interface design (a) Exploded view of the LED-based optical probe showing its main components; (b) Schematic model of the probe with cross-section AA´ illustrating substrate metallization, via and underfill in (c); (d) Probe interconnection to a flexible PI cable, with enlarged schematic cross-section.

This work proposes a modular approach to realizing penetrating neural probes with integrated LEDs. Instead of processing LED epilayers (Goßler et al. 2014) (Scharf et al. 2016; Wu et al. 2015), commercially available LED chips (TR2227 CREE Durham, NC) were chosen for this probe design. The bare LED chips are based on highly efficient indium gallium nitride (InGaN) junction on silicon carbide substrates. Both of their 1-µm-thick contact pads lie on the same side with a chip footprint of 270×220 μm^2 and a thickness of 50 µm. They are integrated into penetrating probes using standard processes for Si- and polymer-based MEMS. Fig. 2a shows an exploded view of the probe, along with a schematic assembled probe in Fig. 2b. The probe is based on a 10-µm-thick double-metal polyimide (PI) substrate electrically interfacing the bare LEDs chips and a ladder-like stiffening structure made of Si surrounding the flip-chip bonded LED chips. Thereby a relatively thin probe cross-section defined mainly by the LED thickness is achieved. The stiffening structure makes the top surface smoother, thus helping to avoid tissue damage which would otherwise be caused by the 50-µm-thick LED chips protruding from the surface of the 10-µm-thick PI substrates. Although the overall width of the probe is increased by 15 µm on each side of the LED chips, thereby slightly increasing bulkiness of the probe by less than 15%, its height is not enlarged by the Si stiffener. The stiffening structure also provides an adequate mechanical stiffness for probe implantation. Cross-section AA´ in Fig. 2c illustrates the PI substrate with the integrated LED wiring, an LED flip-chipped onto and connected to an LED bond pad at the PI substrate surface, and the Si stiffener. Once assembled, the probe has a cross-sectional area of 250×65 μm^2. As requested by our neuroscientific partners, the devices were designed in shank lengths of 5 mm and 8 mm, while the LED pitch is 300 µm and 500 µm with the lower value limited by the dimensions of the LED chips. As illustrated in Fig. 2d, the probes are interfaced with external instrumentation via a flexible PI cable bonded to the probe base. The cable itself is plugged into a mini zero-insertion-force (mini-ZIF) connector on a LED driver circuit for probe operation. The LEDs are controlled by a current driver chip in combination with an Arduino nano microcontroller (Genuino re-seller, Germany).

2.2 Probe fabrication

Double-metal polyimide substrates

The process for realizing the PI-based probe substrates is illustrated in Fig. 3a. Unlike the standard single-metal PI process (Kisban et al. 2009) used by us previously, a double-metal process was established in the scope of this study. Its main fabrication steps were succinctly described previously (Ayub et al. 2015) and are reported in more detail here. The process starts with a 5-µm-thick PI layer (U-Varnish S, UBE Industries Ltd., Tokyo, Japan) spin-coated onto a blank Si carrier wafer (Fig. 3a-i). This is followed by the deposition of a seed layer made of chromium (Cr, 30 nm), gold (Au, 200 nm) and titanium (Ti, 30 nm) for the subsequent electroplating, which thickens the LED interconnection lines and lowers their electrical resistance. While Cr improves the adhesion to the underlying PI layer, Ti serves as an adhesion promoter for the photoresist (PR) AZ9260 (Microchemicals GmbH, Ulm, Germany) used during

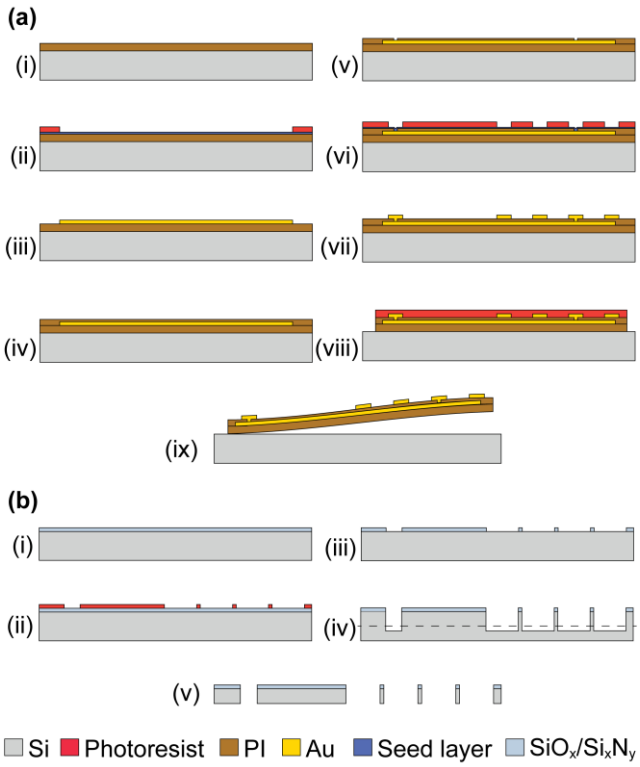

Fig. 3: Fabrication process: Schematic cross-section of the process steps for (a) the 10-µm-thin flexible probe substrates, and (b) the Si stiffener.

electroplating. After patterning the PR, the exposed Ti is selectively removed by wet etching (Fig. 3a-ii). Hence the Au electroplating starts directly on the Au film of the seed layer sandwich. The 10-µm-wide tracks of the LED wiring (cf. cross-section in Fig. 2b) are electroplated to a thickness of 1 µm (Fig. 3a-iii). Thereafter, the seed layer beside the Au tracks is removed using mask-less wet etching of Ti, Au and Cr. For the second PI layer, polyimide is diluted with N-Methyl-2-pyrrolidone (NMP) in a ratio of 3:1 to achieve a PI layer thickness of 2.5 µm, which achieves a lower electrical resistance of the via between metal wiring and the forthcoming metal pads. After spin-coating and curing (Fig. 3a-iv), this thinner PI layer is structured using reactive ion etching (RIE) to realize vias between the two metal levels (Fig. 3a-v). A second seed metal sandwich of identical composition as the first is then sputter deposited (Fig. 3a-vi), followed by Ti patterning, Au electroplating to a final thickness of 3 µm, and again selective removal of the superfluous seed layer. The second electroplating realizes the LED bonding pads and the contact pads at the rear of the substrate to electrically interface the optical probes to the external instrumentation (Fig. 3a-vii). Finally, probe shapes are defined by RIE process using PR as the masking layer (Fig. 3a-viii). The probe substrates are individually peeled off the carrier wafer with the help of tweezers, as illustrated in (Fig. 3a-ix).

Silicon stiffening structures

The probe stiffener, schematically shown in Fig. 2a, is a ladder-like structure realized using 4-inch Si wafers. The fabrication sequence starts with the deposition of a 1-µm-thick, stress compensated silicon oxide (SiO_x)/silicon nitride (Si_xN_y) layer stack using

plasma enhanced chemical vapor deposition (PECVD) (Fig. 3b-i). This is similar to the standard fabrication process of Si probes used by our group (Herwik et al. 2009). The dielectric layers are then patterned and etched by RIE, hence defining the mask against the subsequent deep reactive ion etching (DRIE) of Si (Fig. 3b-ii, -iii). The mask design contains the rectangular windows for the LEDs within the rectangular probe shape terminated by a sharp tip designed to facilitate probe insertion into neural tissue. DRIE is carried out to a depth of 70 µm (Fig. 3b-iv). Finally, the wafer is ground to the required remaining thickness of 40 µm, thus completing this etching-before-grinding process (Herwik et al. 2011). The Si stiffeners were designed with tolerances of 6 µm to accommodate the alignment inaccuracy of the LED assembly on the PI substrates and dimensional variations of the LEDs. Si stiffeners are picked up from the grinding tape with the help of tweezers.

2.3 Device assembly and characterization

Device assembly is delicate in terms of the alignment accuracy of the LED substrate bonding as well as the final mounting of the stiffener on PI substrates containing up to 10 LEDs. In a first step, the bare LED chips are bonded onto the PI-based probe substrate using a flip-chip (FC) bonder (Fineplacer 96λ, Finetech, Berlin, Germany). For this purpose, flexible PI substrates are peeled off the carrier wafer and fixed on a custom designed Si vacuum chuck. Then, LED chips are individually picked up by the bonding tool, aligned with respect to the electroplated bonding pads and bonded using ultrasonic power, force and temperature. After FC bonding, the probe is connected to a flexible PI cable designed to fit to the contact pads on the probe base. The flexible PI cable fabrication essentially follows an established process (Kisban et al. 2009), apart from the fact that the wiring is electroplated to a thickness of 1 µm, again in order to reduce the line resistance. Both PI-based components are aligned and FC bonded, as schematically shown in Fig. 2d, using ultrasonic power, force and temperature. The bonding process was optimized with regards to the electrical resistance of the probe-

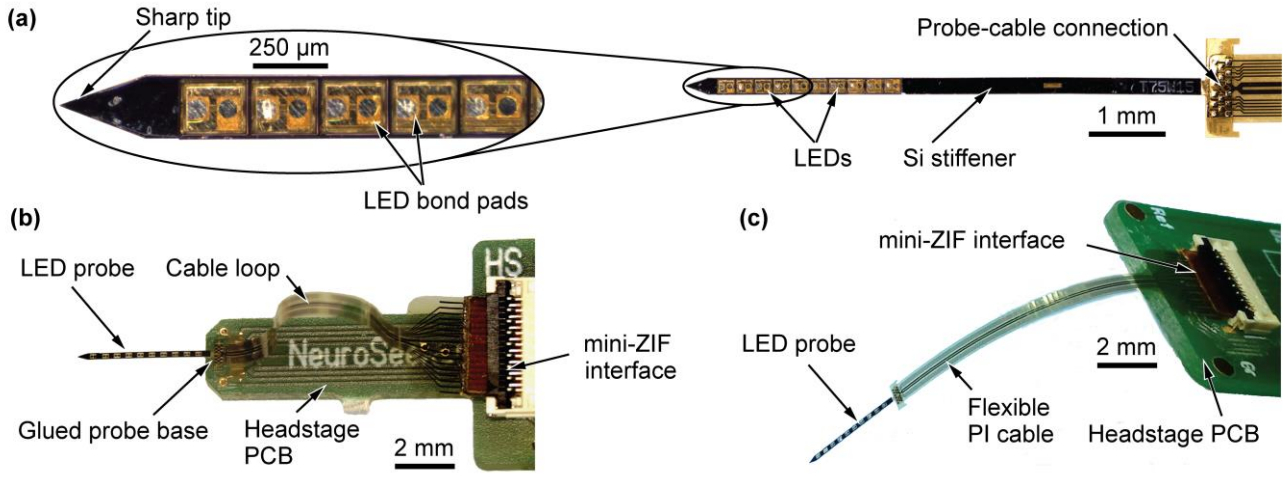

Fig. 4: Device assembly and interconnection (a) Assembled 8-mm-long probe with its cable and a close-up micrograph showing the ladder-like Si stiffener and LEDs inserted into the stiffener cavities. (b) Acute probe variant with the probe adhesively bonded to a printed circuit board (PCB), and, (c) chronic variant of the optical probe connected to a highly flexible PI cable.

cable contact by using dedicated test structures enabling a four-point resistance measurement of the bonded structures.

Next, the roughly 3-µm-high gap between the LED chips and the PI substrate is underfilled using a fluoropolymer (CYTOP 809-M, Asahi Glass Co., Ltd., Japan). Similarly, the probe-cable interface is underfilled as well, thereby increasing the mechanical stability between the two PI components. To further strengthen the adhesion between PI and CYTOP, probe-cable assemblies were subjected to a 5-min oxygen plasma at 50 W (Pico low-pressure plasma system, Diener electronic GmbH, Germany) in order to activate the PI surfaces prior to the application of CYTOP. This intermediate plasma treatment resulted in a pronounced improvement of the system stability later when operated in saline solution. Thereafter, the silicon stiffener is manually fixed on the LED array such that the LED chips fit into the slightly larger stiffener cavities. CYTOP is applied again, now serving as the adhesive keeping the stiffener in place. Assembled probes, as shown in Fig. 4a, are then cured according to the thermal profile suggested by the manufacturer, with a maximum temperature of 120°C applied for 3 hours. The assembled probes undergo a further passivation comprising plasma surface activation, dip coating in CYTOP and a final curing in order to enhance their resistance against saline solution. The assembled optical probes are glued to rigid carriers as shown in Fig. 4b, for acute neuroscientific experiments. On the other hand, Fig. 4c illustrates the device meant for chronic application scenarios, where the flexible PI cable contributes mechanical de-coupling from the probe itself.

Optoelectronic measurements were carried out on assembled probes using an integrating sphere with spectrometer (ISP-50-I-USB, Ocean Optics, Ostfildern, Germany) to determine the optical output power of the LEDs. The LEDs were driven with current source modulating at 30 kHz and a duty cycle of 10 %, i.e. a pulse width of 3.3 µs. The mid-term stability of the devices was investigated using a worst-case scenario by applying a constant bias voltage of –5 V across the LED terminals while exposing the optical probe to 1 M Ringer's solution at room temperature. The chosen constant reverse voltage is approximately twice the forward bias potential requested to operate the LED under normal conditions and therefore creates an accelerated failure condition for the encapsulation. Moreover, the reverse leakage current through the device can be distinguished easily from the forward current which is influenced by the temperature increase. The leakage current between the LED terminals is registered at intervals of 10 s until it crosses a limit set at 100 µA.

2.4 Acute surgery and electrophysiological recordings

(a) Experiment I – Thalamic stimulation and cortical recording

The LED-based optical probes were validated in two in vivo experiments. In the first study carried out at the Research Centre for Natural Sciences of the Hungarian Academy of Sciences, the experiments were performed according to the EC Council Directive of November 24, 1986 (86/89/EEC) with all procedures being reviewed and

approved by the local ethical committee and the National Food Chain Safety Office of Hungary (PEI/001/2290-11/2015). Implantations were done under general anesthesia where two adult male mice (vesicular-GABA transporter-channelrhodopsin-2 (vGAT-ChR2), weight: 25 g to 35 g) received an intraperitoneal injection of urethane (1.5 mg/g). The body temperature of the animals was maintained during the experiments at 37 °C using a thermostatically regulated heating pad (RWD, China).

Mice were placed in a stereotaxic frame (David Kopf Instruments, Tujunga, CA, USA) and two craniotomies were made with a dental drill, one for the recording probe (2×2 mm^2) and one for the optical probe (2×2 mm^2). Stereotaxic coordinates were used to determine the cortical location for recording (anterior-posterior (AP): –0.3 mm; medial-lateral (ML): 3 mm from the bregma) and the thalamic location for optical stimulation (AP: –1.5 mm; ML: 1.8 mm from the bregma) (Paxinos and Franklin 2001). A single-shank silicon probe with 16 recording sites with a site spacing of 100 µm (A1×16-5mm, NeuroNexus Technologies, Ann Arbor, MI, USA) was attached to a micromanipulator, moved over the targeted brain location and inserted slowly into the barrel cortex of the animal to a depth of 1.1 mm. One optical probe with 300 µm LED pitch as described in Sect. 2.3 was attached to another micromanipulator and implanted into the thalamus, penetrating through the ventrobasal complex and the nucleus reticularis thalami (nRt), to a depth of 4.3 mm. The LED at the bottom of the probe shaft (LED1) was located beneath the thalamus, while some of the LEDs (LEDs 7-10) were located above the thalamus. The LEDs were facing the medial side of the brain. A schematic illustration of the stimulation and recording sites for our experiment is shown in Fig. 5a, b.

The Si-based recording probe was connected to an electrophysiological recording system (RHD2000, Intan Technologies, Los Angeles, CA, USA) comprising a 32-

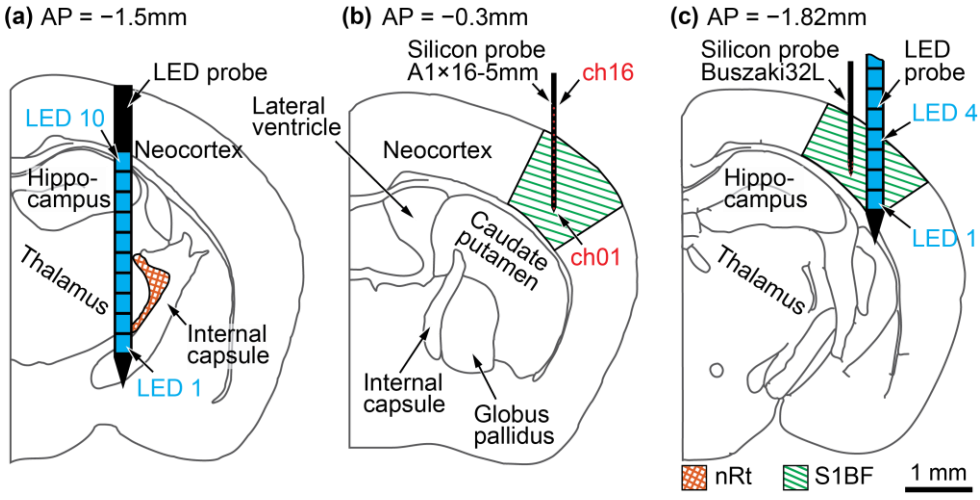

Fig. 5: Schematic representation of the experimental configurations showing (a) thalamic location of the optical probe and (b) cortical position of the recording probe in the mouse brain as applied in in Experiment I. The recording probe covered several layers of the barrel cortex (S1BF) while using bottom six LEDs in the nucleus reticularis thalami (nRt) for optical stimulation. (c) The optical and recording probes of Experiment II were positioned approx. 200 to 400 µm away from each other in the somatosensory cortex, with bottom four LEDs inside the brain tissue.

channel headstage. Brain activity was recorded on 16 channels with 16-bit resolution at 20 kHz sampling rate. A stainless-steel wire inserted into the neck muscle of the animal served as the reference and ground electrode. The wideband traces of electrical activity (0.1 to 7500 Hz) were filtered (500-5000 Hz bandpass filter, zero-phase shift, 24 dB/octave) to obtain the multi-unit activity (MUA). Neural responses to optical stimuli were averaged to extract the mean evoked responses.

The optical probe was inserted directly into the thalamus and 20-ms-long light pulses of 20 µW and 1 mW were delivered with an interstimulus interval (ISI) of 4 s. During the optical stimulation, LEDs were operated sequentially, i.e. only one LED at a time, starting from the LED1 located at the tip of the probe followed by the adjacent LED located dorsally. The delivery time of light pulses was recorded on a trigger channel, while the duration and the ISI of the light pulses was controlled with a RP2 Real-Time Processor (Tucker-Davis Technologies, Alachua, FL, USA). The spatial sequence of consecutive pulses to operate the LEDs and the light intensity was modulated using an Arduino nano micro-controller board in addition to the LED driver circuit.

(b) Experiment II – Cortical stimulation and inhibition

In the second study carried out at INSERM, University of Lyon 1, all procedures were approved by the institutional animal care and use committee of the university (Protocol DR2013-47) and were conducted in accordance with the French and European Community guidelines for the use of research animals. Recordings were performed in mice under urethane anesthesia (1.7 mg/g) with the body temperature being maintained at 37 °C with a heating blanket. All animals used in this study were maintained on a C57Bl6 genetic background and group-housed in the vivarium under normal light cycle conditions.

We used heterozygous male offsprings of GAD2-ires-Cre driver mice (010802, Jackson) crossed with Ai32 {RCL-ChR2 (H134R)/EYFP} reporter mice (012569, Jackson) where ChR2 is found selectively in GABAergic inhibitory neurons. On the day of recording, mice (6-12 weeks old) were implanted with a lightweight metal head holder and a recording chamber under deep isoflurane anesthesia. Small epidural ground and reference screws were positioned over the cerebellum. A small craniotomy (1.5-2 mm diameter) was performed above the primary somatosensory cortex (S1). A 5-mm-long optical probe with 300 µm LED pitch was lowered vertically into the

Table 1: Experimental contact resistance values (mean and standard deviation (SD)) evaluated using dedicated test structures.

No.	Resistance in mΩ (mean±SD)
1	6.175 ± 0.309
2	9.225 ± 1.138
3	10.175 ± 1.162
4	11.25 ± 0.9

cortical tissue until 4 of 10 LEDs were inside the brain, covering all cortical layers. A 10-mm-long 32-channel silicon recording probe with four shanks interspaced by 200 µm (Buzsaki32L-CM32, NeuroNexus Technologies) was slowly lowered into the neighboring tissue (200 µm to 400 µm away from the optical probe) to search for single-unit signals (Fig. 5c). The implantation depth of the silicon probe was measured from the cortical surface based on the distance of the recording sites from the tip, which is 50 µm. Signals were acquired at 20 kHz with a 32-channel data acquisition system (ME32-FAI-µPA, Multi-Channel Systems MCS GmbH, Germany). Light stimulation was applied through the sequential activation of each LED with 1-s-long pulses every 5 s with an optical power of 17 µW.

Spike sorting was performed with the Klustakwik software suite (Harris et al. 2000). Putative GABAergic fast-spiking neurons (expressing ChR2) were identified on the basis of their action potential (AP) waveforms and auto-correlograms. Control firing rates were computed from the 2 s period immediately preceding light activation. All values are presented as mean ± standard error of mean (SEM) unless otherwise stated. Statistical comparisons between firing rate responses were performed using the Mann-Whitney U test.

3 RESULTS

3.1 Electrical and Optical measurements

Probes were characterized both optically and electrically prior to their application in one of the in vivo experiments. As a first example, Fig. 6a demonstrates the individual control of LEDs integrated on a probe with an inter-LED pitch of 300 µm. Representative *I-V* curves of LEDs on an assembled probe indicate a line resistance of 24 Ω. This is calculated by comparing the *I-V* curves of a bare LED chip with those bonded on an assembled probe, as shown in Fig. 6b. Moreover, dedicated test structures were used to extract the contact resistance of the cable-probe interfaces. The respective values of the contact resistances measured using the four-point method for $n = 4$ structures realized on different fabrication wafers are listed in Tab. 1, indicating values below 12 mΩ per contact.

Since the PI substrate is semitransparent, light is emitted from both sides of the probe. However, because of the Si stiffener, the radiant flux is reduced by 40 % compared to a bare LED chip mounted on a PI substrate without the stiffener. Fig. 6c shows the measured optical output power of individual LEDs as a function of driving current (for experimental details, see Sec. 2.3). At forward currents of 10 mA with a duty cycle of 10%, the probes are capable of delivering more than 500 µW of optical radiant power into the brain tissue. Furthermore, the mid-term accelerated failure test suggests that the probes are suitable for acute experiments lasting several hours. This is illustrated in Fig. 6d, where the passivation of the devices holds up for up to 6 hours, under the test conditions mentioned earlier. The passivation layer adds up 4.19±1.28 µm (mean±SD) to the total thickness of the probes.

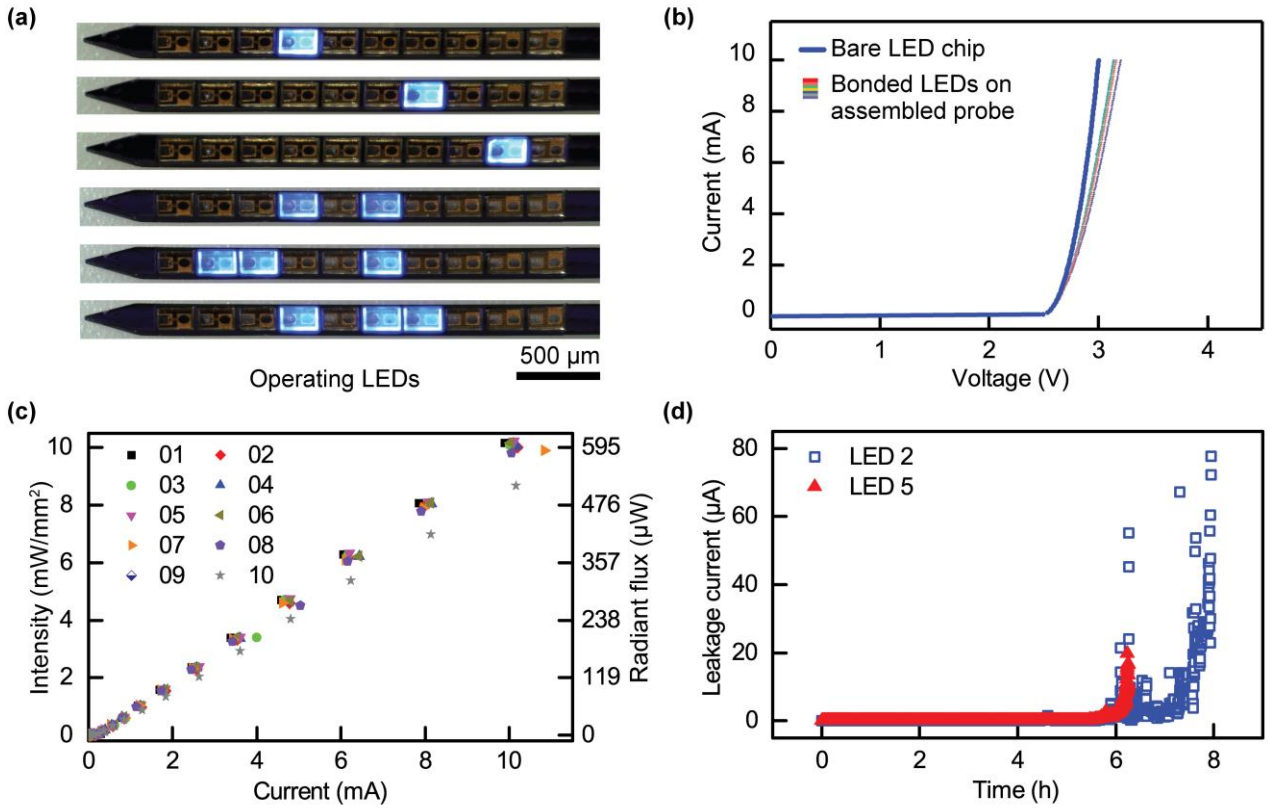

Fig. 6: Optoelectronic measurements (a) Optical micrographs demonstrating the operation of individual and multiple LEDs; (b) *I-V* characteristics of bonded LEDs measured on an assembled probe with a 40-mm-long cable in comparison with a bare LED chip; (c) Intensity, i.e., optical power per LED area, for all 10 LEDs along a probe shank; operating conditions are 30 kHz and 10 % duty cycle; (d) Probe stability assessed using the reverse leakage current between LED terminals, with the optical probe immersed in Ringer's solution.

3.2 Acute in vivo probe validation

(a) Experiment I – Modulation of cortical activity by optogenetic stimulation of thalamic neurons

The acute experiments were performed as a proof of concept of these innovative optical devices. In the mouse strain (vGAT-ChR2) selected for the first experiments, ChR2 is expressed in the somata and axonal terminals of GABAergic neurons of the nucleus reticularis thalami (nRt). In this mouse model, optogenetic stimulation can be used to selectively drive the nRt to generate sleep spindles (brief epochs of oscillations with a characteristic frequency range of 7-15 Hz) in the neocortex (Halassa et al. 2011). In order to test the functionality of the optical probe, the device was implanted into the thalamus of the animal. A silicon-based linear multi-electrode array was implanted beside the optical probe as explained earlier, into the primary somatosensory cortex to record optically evoked neuronal activity. Using brief light pulses delivered to the thalamus, we could reliably evoke spindles in the cortex, as shown in Fig. 7a, c. Optically driven spindle generation depends on the state of the anesthesia which can only be evoked during light anesthesia, where sleep spindles occur spontaneously. During deep anesthesia, instead of spindles, up-states could be evoked by optical

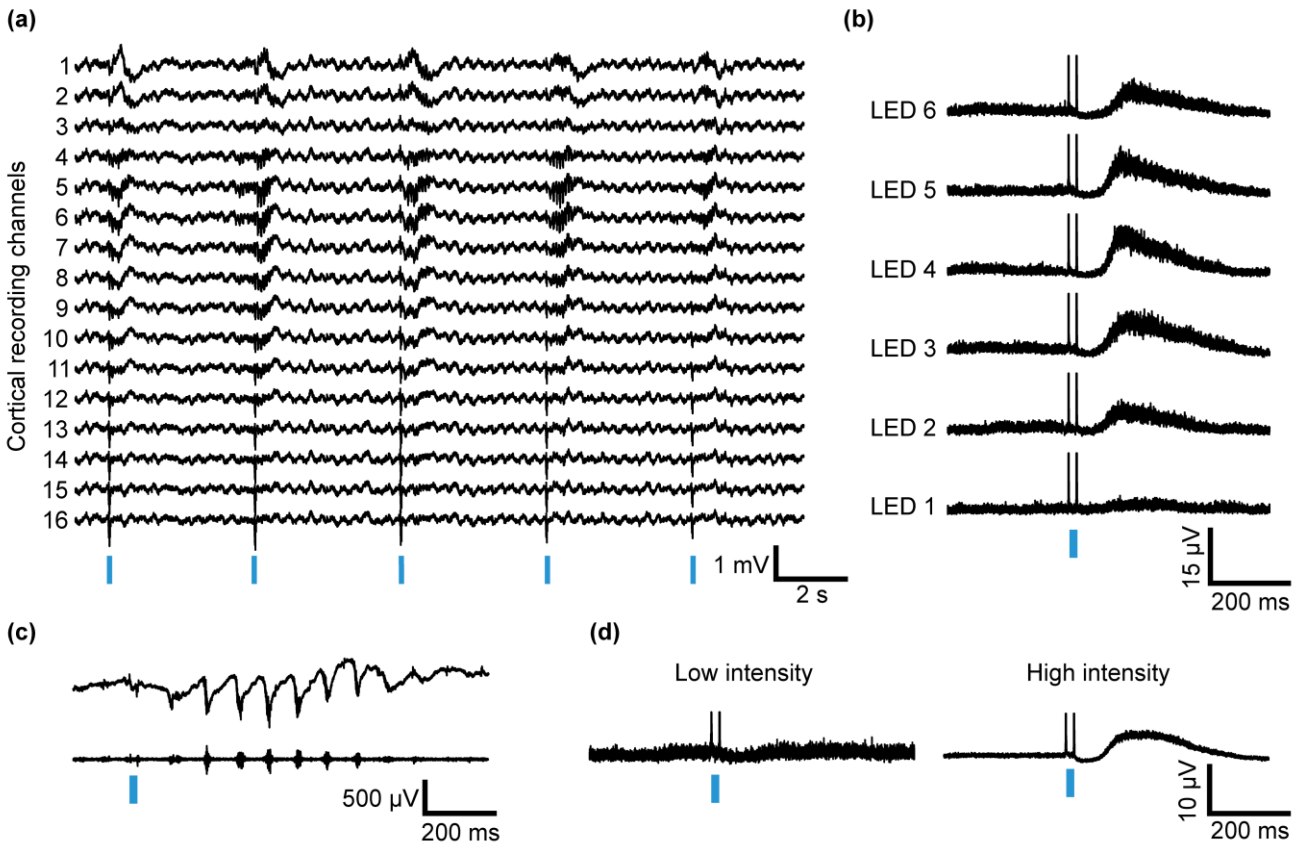

Fig. 7: Sample results of in vivo experiments performed with the LED-based optical probe (a) Raw traces recorded with a 16-channel silicon probe from the somatosensory cortex of a urethane-anesthetized transgenic mouse. Optogenetic stimulation of the soma or axon terminals of nRt neurons could reliably evoke sleep spindles. The delivery time of 20-ms-long light pulses is indicated by the blue bar. The high amplitude spikes appearing in the recordings at the beginning and end of light pulses are electromagnetic artefacts caused by switching the LED from an off-state to the on-state and vice versa. (b) Average cortical MUA responses on Channel 2 to light pulses delivered by six different LEDs. Only one LED was active at the same time. Based on the implantation depth, LED 1 was located most ventrally in the brain tissue, at the bottom of the thalamus, while LED 6 was located at the top of the thalamus. Note the different amplitudes and latencies of the evoked responses to the optical stimulation with different LEDs. (c) Representative evoked sleep spindle at a faster time scale. Wideband activity (top) and multi-unit activity (MUA, bottom) recorded on Channel 5. (d) Average of cortical MUA responses recorded on Channel 2 to LED pulses delivered with low intensity (left) and high intensity (right).

stimulation, which are the active phases of the slow (<1 Hz) thalamocortical oscillation (Neske 2016).

To test the effect of different light intensities on the evoked neural responses, we delivered low- and high-intensity light pulses with the same LED located in the thalamus. Subthreshold light pulses with low optical intensity at ~20 µW did not evoke any detectable MUA, while higher intensity light pulses at ~1 mW resulted in a brief initial decrease of neuronal activity followed by a strong activation, as shown in Fig. 7d. Stimulating different sections of the thalamus with LEDs located at different depths showed diverse neural responses (Fig. 7b). Typically, optical stimulation in the thalamus resulted in an initial inhibition of cortical spiking activity during the first 50 ms, followed by a strong neural activation slowly returning to the baseline after 400 ms. To quantify the differences between responses evoked by the activation of

Table 2: Extracted attributes of the averaged cortical MUA response evoked by activating LEDs located at different depths (Fig. 7b) characterizing the depth-dependent stimulation of the nRt thalamic nucleus. The mean MUA response was filtered (100 Hz low-pass filter, zero phase-shift, 24 dB/octave) and baseline corrected before obtaining the four values. The attributes are defined in the main text.

	LED 1	**LED 2**	**LED 3**	**LED 4**	**LED 5**	**LED 6**
Inhibition amplitude (µV)	–0.22	–0.86	–1.45	–1.45	–1.15	–1.53
Onset latency (ms)	52.85	75.65	81.85	83.55	83.40	101.55
Peak amplitude (µV)	1.70	4.90	7.70	9.80	8.30	5.40
Peak latency (ms)	190.90	130.60	145.10	141.30	128.70	148.80

LEDs located at different depths, we calculated the following attributes of the averaged cortical MUA response:

- *Inhibition amplitude*, i.e., mean amplitude during the initial inhibition period calculated in the 30-50 ms time period after the stimulus onset,
- *Onset latency*, i.e., latency of the neural activity returning to the baseline (0 µV) after the initial inhibition period,
- *Peak amplitude*,
- *Peak latency*, i.e., latency of peak amplitude

The obtained values are summarized in Table 2. The mean MUA response to the stimulation with light pulses emitted by LED 1 located most ventrally in the brain tissue, showed only a subtle initial inhibition peak and a small peak amplitude with an early onset and a delayed peak latency compared to the MUA responses evoked by light pulses located more dorsally. Based on the anatomical coordinates of the implantation site, as illustrated in Fig. 5, LED 1 was located below the nRt which explains the observed weak response. Light pulses emitted by LEDs above LED 1, i.e. LED 2 to LED 4 produced responses with gradually increasing initial inhibition, onset latency, peak amplitude, and a peak latency in the 130-150 ms range. These observations suggest that more and more neurons get involved in the stimulus processing as LEDs located more dorsally are activated. By activating LED 5, the inhibition became slightly weaker and the peak amplitude smaller compared to the extreme values seen in the response to a stimulation with LED4. Using LED 6, which was located near the top of the nRt, the peak amplitude of the evoked response was even smaller. However, the initial inhibition was very strong and, based on the higher onset and peak latencies, it lasted even longer than the inhibition observed by activating LEDs located more ventrally. The observed results prove that a depth-dependent modulation of cortical activity is possible with our probes. Furthermore, our findings suggest that the observed cortical MUA response depends presumably on the amount and location of stimulated nRt cells.

(b) Experiment II – Cortical layer specific optical stimulation

In order to better characterize the effectiveness of our probes, we performed further experiments by implanting 5-mm-long probes into the somatosensory cortex vertically covering the entire thickness of the cortical tissue. Based on the measured probe depth during each recording session, one LED was determined to face the recording sites of the silicon probe and assigned the name “facing LED”. Neighboring LEDs were then assigned the name “LED +1”, LED +2, etc. Sequential activation of LEDs differently altered the firing rates of single-unit recordings: putative excitatory pyramidal cells (n = 13) significantly decreased their firing activity ($p < 0.01$ for each LED activated compared to the control, Fig. 8) while putative GABAergic fast-spiking neurons (n = 4) increased their firing activity only when the “facing LED” was activated (p = 0.057 (facing LED); p = 0.2 (LED +1); p = 0.17 (LED +2) compared to the control, Fig. 9).

Typically, fast-spiking cells have a somato-dendritic arborization that can span a few hundred microns (Gentet et al. 2010). Our results indicate that light emanating from the facing LED was spatially restricted and did not significantly impact a channelrhodopsin-expressing (putative cortical GABAergic cell) neuron located

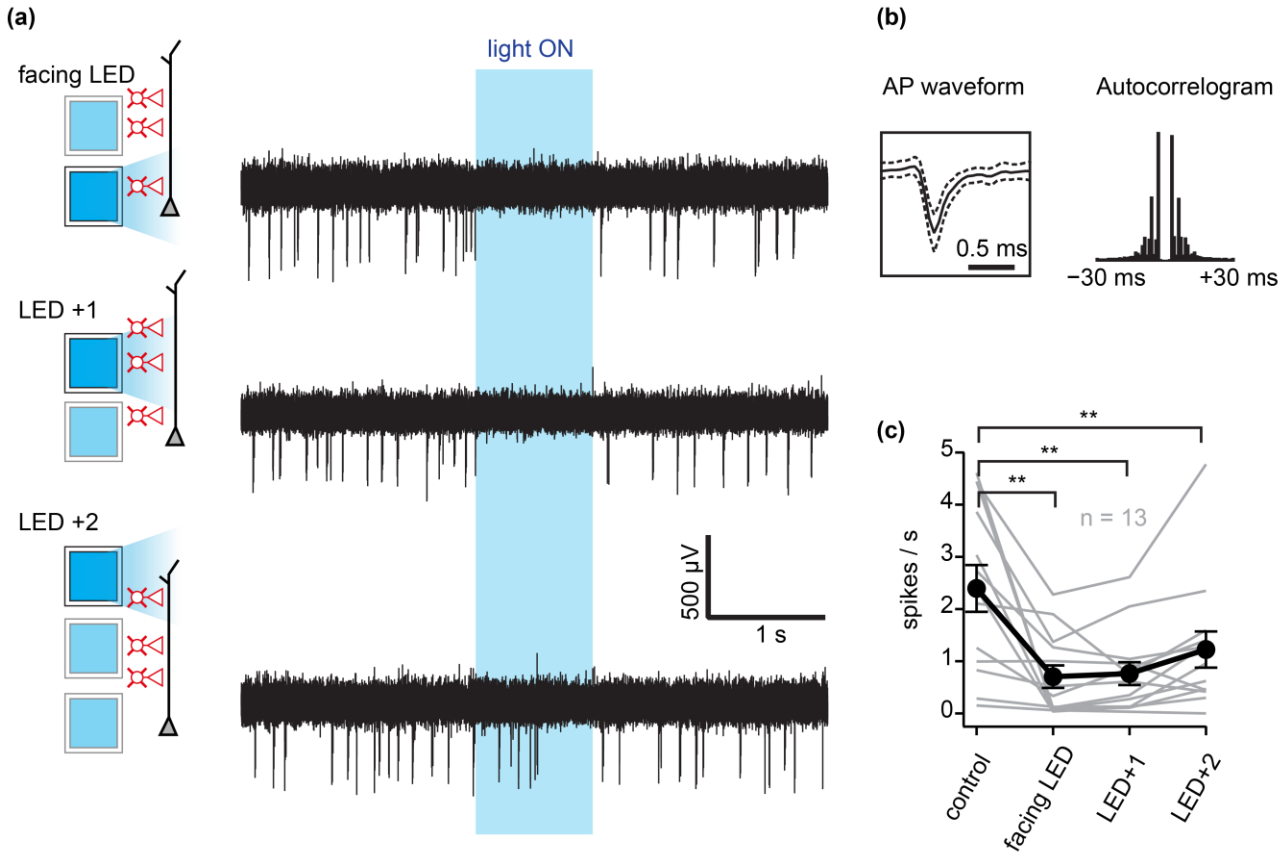

Fig. 8: Depth-independent optogenetic inhibition of cortical excitatory neurons in vivo. (a) Sequential activation of LEDs decreases the electrical activity of extracellularly-recorded regularly spiking (RS) putative excitatory neurons. Schematic illustration of the anatomical configuration of activated LEDs and the recorded cell (left) together with representative recording traces from the putative excitatory neuron (right). LEDs are activated for 1 second during the recording (blue background). (b) Average spike waveform and autocorrelogram from the same cell as in (a). (c) Average firing rates from n = 13 putative excitatory neurons in control vs. each LED activation.

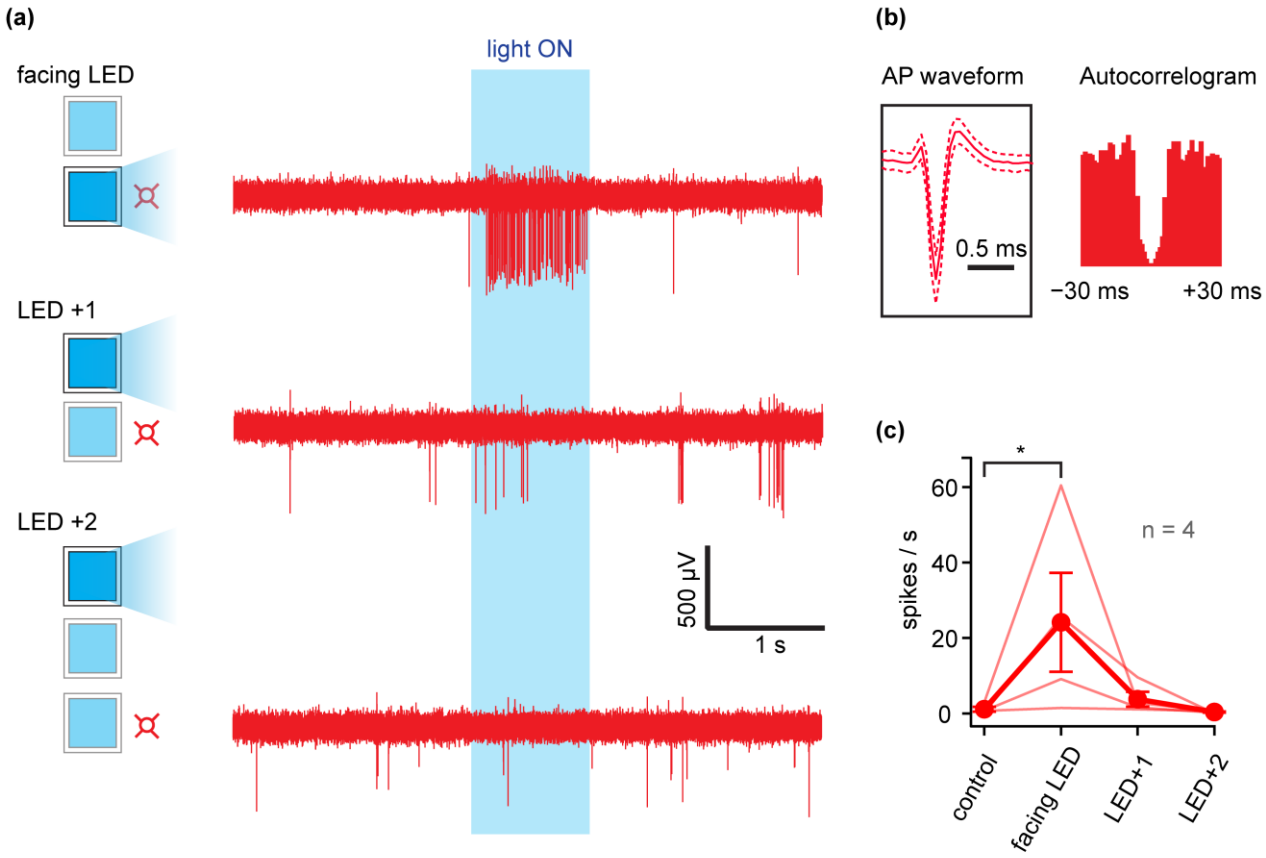

Fig. 9: Depth-dependent optogenetic activation of PV+ neurons in vivo. (a) Sequential activation of LEDs increases the electrical activity of extracellularly-recorded fast-spiking PV+ neurons expressing ChR2. Schematic illustration of the anatomical configuration of activated LEDs and the recorded cell (left) together with representative recording traces from the PV+ neuron (right). LEDs are activated for 1 second during the recording (blue background). (b) Average spike waveform and autocorrelogram from the same cell as in (a). (c) Average firing rates from *n* = 4 PV+ neurons in control vs. each LED activation.

distally at distances larger than the LED pitch. On the other hand, pyramidal neurons, especially bitufted cells from Layer 5, have extensive somato-dendritic arborizations that can span all the way to the cortical surface and are contacted by GABAergic cells (Fig. 8a) located throughout Layers 1-6 at different synaptic points along their arborizations (Ramaswamy and Markram 2015).

4 CONCLUSION

We have presented a modular approach to realize intracerebral neural probes with integrated LEDs as light sources. As demonstrated, these optical probes enable a depth-dependent optical stimulation of neural activity. On the one hand, the use of the Si stiffener ensures an improved probe rigidity for implantation in cerebral tissue, while on the other hand, it renders the probe surface relatively smooth despite the fact that LEDs protrude by 50 µm from the surface of the PI substrate. This is expected to minimize tissue response in comparison with devices with more rugged topography (Cao et al. 2013). The implementation of commercial bare LEDs rather than custom-made devices leads to a pronounced decrease in development time and fabrication cost

compared to more advanced approaches using thin-film LED technologies (Ayub et al. 2016; Goßler et al. 2014; Scharf et al. 2016; Wu et al. 2015). Despite the larger surface area of these probes with a cross-sectional area of 250×65 µm^2, in comparison to probes implementing thin-film LEDs, with cross-sections down to 70×30 µm^2 (Wu et al. 2015), an electrical to optical conversion efficiency of a better 17 % is achievable for optical stimulation. When the LEDs are operated as current driven devices, their temperature increase during operation is a major concern for neuroscientists. As demonstrated for an optical fiber-based light delivery device to be placed on the brain surface, the temperature increase of the device surface can be kept below 2 K by using pulse-width modulation (PWM) of the LED current of 30 mA at a duty cycle of 10% and a peak electrical power P_{el} = 125 mW (Schwaerzle et al. 2015). The time-averaged optical radiant flux of 1 mW/mm^2 of that device is limited in this case mainly by the inefficient light coupling between LED and optical fiber. In contrast, the presented LEDs are intended for a local intervention in brain tissue. If operated at 1.24 mA, i.e., at a roughly 25 times lower current, corresponding to P_{el} = 3.35 mW, the LED delivers an optical power of P_{opt} = 59 µW (cf. Fig 6b, c), equivalent to a radiant flux density of 1 mW/mm^2. In view of the significantly lower dissipated electrical power, we expect a similar reduction of the average temperature increase of the LEDs, e.g. about 0.05 K. Even at an optical power of 500 µW, as mentioned in Sect. 3.1, corresponding to a current of 10 mA (cf. Fig. 6c) and P_{el} = 31.7 mW, the temperature increase is consequently estimated to be below 0.5 K. Data of a previous study (Scharf et al. 2016) lead to the conclusion that the peak temperature increase converges to the average temperature increase at higher pulse frequencies. This is already evidenced by the data achieved at 100 Hz. Since we operate our LEDs at 30 kHz, we expect peak temperature to hardly exceed the average temperature.

Additionally, the experience of end users highlights the robust probe interface technique allowing at times a rough handling of these devices and offers flexibility to in view of their experimental setups. The probes were shown to exhibit an acceptable stability under operating conditions harsher than during realistic experimental situations. Hence the optical probes are concluded to be applicable for safely carrying out acute in vivo experiments, which is corroborated by the multiple in vivo experimental studies presented here. However, critical inspection revealed that CYTOP leaves trapped air underneath the LEDs while its solvent evaporates during the curing phase. Further work related to the probe encapsulation aims at finding alternative ways to address the LED underfilling (Raz et al. 2016). Using these optical probes, we demonstrated the manipulation of neural activity in transgenic mice expressing ChR-2. The ability to simultaneously record electrical activity and stimulate the brain by blue light pulses with fine temporal and spatial control makes it possible to examine the role of various brain circuits. We observed depth-dependent and light intensity-dependent changes in the firing rate of the recorded neurons, which confirms the functionality of the devices. In a future design revision, the illumination surface area of the LEDs can be reduced using Si stiffening structures with an increased thickness partially extending over the LEDs. This will in addition allow

electrodes to be integrated directly on the probe in the plane of light stimulation, thereby enhancing the probe capability to electrically record neural activity with a precise spatial control.

Acknowledgement

The research leading to these results received funding from the European Union's 7th Framework Program (FP7/2007-2013) under grant agreement n°600925 (NeuroSeeker), the *BrainLinks-BrainTools* Cluster of Excellence funded by the German Research Foundation (DFG, grant no. EXC 1086), and the Hungarian Brain Research Program (Grant Nos. KTIA-13-NAP-A-IV/1-4,6).

References

A. P. Alivisatos, A. M. Andrews, E. S. Boyden et al., ACS Nano **7**, 1850 (2013).

M. T. Alt, E. Fiedler, L. Rudmann, J. S. Ordonez, P. Ruther, and T. Stieglitz, Proc. IEEE **105**, 101 (2017).

S. Ayub, C. Gossler, M. Schwaerzle, E. Klein, O. Paul, U. T. Schwarz, and P. Ruther, in 29th IEEE Int. Conf. Micro Electro Mech. Syst. (IEEE, 2016), pp. 379–382.

S. Ayub, M. Schwaerzle, O. Paul, and P. Ruther, in Procedia Eng. (Elsevier B.V., 2015), pp. 472–475.

E. S. Boyden, F. Zhang, E. Bamberg, G. Nagel, and K. Deisseroth, Nat. Neurosci. **8**, 1263 (2005).

H. Cao, L. Gu, S. K. Mohanty, and J.-C. Chiao, IEEE Trans. Biomed. Eng. **60**, 225 (2013).

F. H. C. Crick, Sci. Am. **241**, 219 (1979).

L. J. Gentet, M. Avermann, F. Matyas, J. F. Staiger, and C. C. H. Petersen, Neuron **65**, 422 (2010).

C. Goßler, C. Bierbrauer, R. Moser, M. Kunzer, K. Holc, W. Pletschen, K. Köhler, J. Wagner, M. Schwaerzle, P. Ruther, O. Paul, J. Neef, D. Keppeler, G. Hoch, T. Moser, and U. T. Schwarz, J. Phys. D. Appl. Phys. **47**, 205401 (2014).

V. Gradinaru, F. Zhang, C. Ramakrishnan, J. Mattis, R. Prakash, I. Diester, I. Goshen, K. R. Thompson, and K. Deisseroth, Cell **141**, 154 (2010).

M. M. Halassa, J. H. Siegle, J. T. Ritt, J. T. Ting, G. Feng, and C. I. Moore, Nat. Neurosci. **14**, 1118 (2011).

T. Hanson, N. Fitzsimmons, and J. O'Doherty, in Methods Neural Ensemble Rec., 2nd ed. (CRC Press, 2007), pp. 47–55.

K. D. Harris, D. A. Henze, J. Csicsvari, H. Hirase, and G. Buzsáki, J. Neurophysiol. **84**, 401 (2000).

S. Herwik, S. Kisban, A. A. A. Aarts, K. Seidl, G. Girardeau, K. Benchenane, M. B. Zugaro, S. I. Wiener, O. Paul, H. P. Neves, and P. Ruther, J. Micromech. Microeng. **19**, 74008 (2009).

S. Herwik, O. Paul, and P. Ruther, J. Microelectromechanical Syst. **20**, 791 (2011).

HyungDal Park, Hyun-Joon Shin, Il-Joo Cho, Eui-sung Yoon, J.-K. F. Suh, Maesoon Im, Euisik Yoon, Yong-Jun Kim, and Jinseok Kim, in Annual Int. Conf. IEEE Eng. Med. Biol. Soc. (IEEE, 2011), pp. 2961–2964.

K. Kampasi, E. Stark, J. Seymour, K. Na, H. G. Winful, G. Buzsáki, K. D. Wise, and E. Yoon, Sci. Rep. **6**, 30961 (2016).

T. -i. Kim, J. G. McCall, Y. H. Jung, X. Huang, E. R. Siuda, Y. Li, J. Song, Y. M. Song, H. A. Pao, R.-H. Kim, C. Lu, S. D. Lee, I.-S. Song, G. Shin, R. Al-Hasani, S. Kim, M. P. Tan, Y. Huang, F. G. Omenetto, J. A. Rogers, and M. R. Bruchas, Science (80-.). **340**, 211 (2013).

S. Kisban, J. Kenntner, P. Janssen, R. V. Metzen, S. Herwik, U. Bartsch, T. Stieglitz, O. Paul, and P. Ruther, in IFMBE Proc. (2009), pp. 107–110.

G. Nagel, T. Szellas, W. Huhn, S. Kateriya, N. Adeishvili, P. Berthold, D. Ollig, P. Hegemann, and E. Bamberg, Proc. Natl. Acad. Sci. **100**, 13940 (2003).

G. T. Neske, Front. Neural Circuits **9**, 88 (2016).

G. Paxinos and K. B. J. Franklin, The Mouse Brain in Stereotaxic Coordinates, 2nd ed. (Academic Press, 2001).

F. Pisanello, L. Sileo, I. A. Oldenburg, M. Pisanello, L. Martiradonna, J. A. Assad, B. L. Sabatini, and M. De Vittorio, Neuron **82**, 1245 (2014).

S. Ramaswamy and H. Markram, Front. Cell. Neurosci. **9**, 233 (2015).

R. Raz, M. Schwaerzle, O. Paul, and P. Ruther, in Optogen B. Abstr. (2016), p. 50.

P. Ruther and O. Paul, Curr. Opin. Neurobiol. **32**, 31 (2015).

R. Scharf, T. Tsunematsu, N. McAlinden, M. D. Dawson, S. Sakata, and K. Mathieson, Sci. Rep. **6**, 28381 (2016).

M. Schwaerzle, P. Elmlinger, O. Paul, and P. Ruther, in 28th IEEE Int. Conf. Micro Electro Mech. Syst. (IEEE, 2015), pp. 162–165.

M. Schwaerzle, O. Paul, and P. Ruther, J. Micromech. Microeng. **27**, 65004 (2017)

T. Stieglitz, M. Schuetter, and K. P. Koch, IEEE Eng. Med. Biol. Mag. **24**, 58 (2005).

M. Wiest, J. Meloy, and E. Thomson, in Methods Neural Ensemble Rec., 2nd ed. (CRC Press, 2007), pp. 97–124.

K. D. Wise, A. M. Sodagar, Ying Yao, M. N. Gulari, G. E. Perlin, and K. Najafi, Proc. IEEE **96**, 1184 (2008).

F. Wu, E. Stark, P.-C. Ku, K. D. Wise, G. Buzsáki, and E. Yoon, Neuron **88**, 1136 (2015).

O. Yizhar, L. E. Fenno, T. J. Davidson, M. Mogri, and K. Deisseroth, Neuron **71**, 9 (2011).

F. Zhang, L.-P. Wang, M. Brauner, J. F. Liewald, K. Kay, N. Watzke, P. G. Wood, E. Bamberg, G. Nagel, A. Gottschalk, and K. Deisseroth, Nature **446**, 633 (2007).